Supplement of Atmos. Chem. Phys., 24, 2399–2414, 2024
https://doi.org/10.5194/acp-24-2399-2024-supplement

Atmospheric Chemistry and Physics
Open Access
EGU

Supplement of

Particle phase state and aerosol liquid water greatly impact secondary aerosol formation: insights into phase transition and its role in haze events

Xiangxinyue Meng et al.

Correspondence to: Zhijun Wu (zhijunwu@pku.edu.cn)

S1. Detailed information of instruments equipped in the air monitoring laboratory

In this study, a weather station (Met One Instruments Inc., USA) was equipped in the laboratory to measure meteorological parameters, including ambient relative humidity (RH), temperature (T), wind speed (WS) and wind direction (WD). Trace gases were recorded using a suite of automatic gas analyzers from Thermo Scientific, including O_3 (model 49i), SO_2 (model 43i), CO (model 48i), and NOx (model 42i). The chemical compositions of non-refractory particles (NR-PM1) were measured by Aerodyne Quadrupole Aerosol Chemical Speciation Monitor (Q-ACSM) equipped with a standard vaporizer. A perma pure nafion dryer was set up in front of the inlet of Q-ACSM to guarantee the RH below 30%. The instrument calibration was operated using pure ammonium nitrate and ammonium sulfate before and after the whole observation to determine the relative ionization efficency followed by the standard protocols (Ng et al., 2011).

S2. Timescales for water diffusion in particles within RH adjustment system

In this study, the characteristic half-time for water diffusion ($\tau_{1/2}$) is employed to give basic information about the timescales for water molecules diffusion into particles in the RH adjustment system. $\tau_{1/2}$ is given by Seinfeld and Pandis (2006) as $\tau_{1/2} = \frac{r^2}{\pi^2 D ln(2)}$, where r is the radius of the particles and D is the water diffusion coefficient. It should be noted that the diffusion timescale within particles is calculated at a constant water activity, meaning that D remains constant as well. An RH of 80% represents the nearly highest RH conditions during our observation, potentially indicating an upper level of the humidification process. For particles with a diameter of 300 nm, $\tau_{1/2}$ was approximately 1.03 seconds. This was calculated using a constant water activity (80% RH) at room temperatures, with the water diffusion coefficient being 10^{-10} m^2 s^{-1} (Koop et al., 2011). Particles with diameter smaller than 300 nm have even shorter water diffusion timescales (e.g., 0.46 seconds for 200 nm particles; 0.11 seconds for 100 nm particles). This is consistent with the laboratory study by Price et al. (2014), which quantified water diffusion in high-viscosity aerosols and determined that water diffusion timescales are less than 1 second for particles with a radius smaller than 250 nm at room temperature. The measured particles were initially dried to ~30% RH before entering the sampling line. However, these particles rapidly reached ambient RH conditions and passed through the RH adjustment system, which had a tested residence time of about 3.3 seconds using a highly humid flow pulse as shown in Fig. S1. Given that the timescales for water

diffusion into particles were much shorter than their residence time, it is presumed that particles rapidly reached equilibrium with the impactor RH during the measurement.

Fig. S1 Time after pulse for RH adjustment system

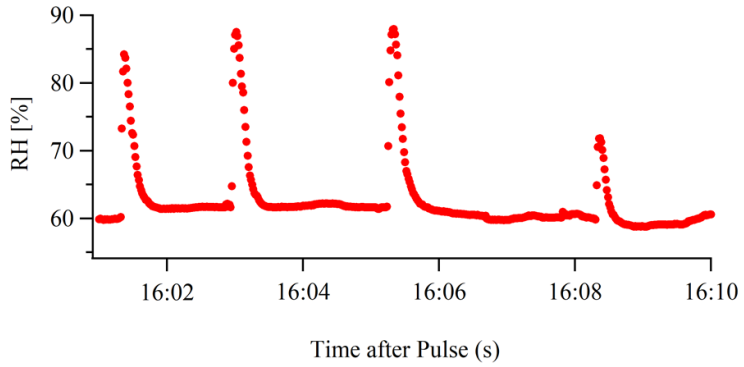

Fig. S1 Time after pulse for RH adjustment system by using humid flow go through the flow path.

Fig. S2 Time series and mass spectral profiles for PMF solution

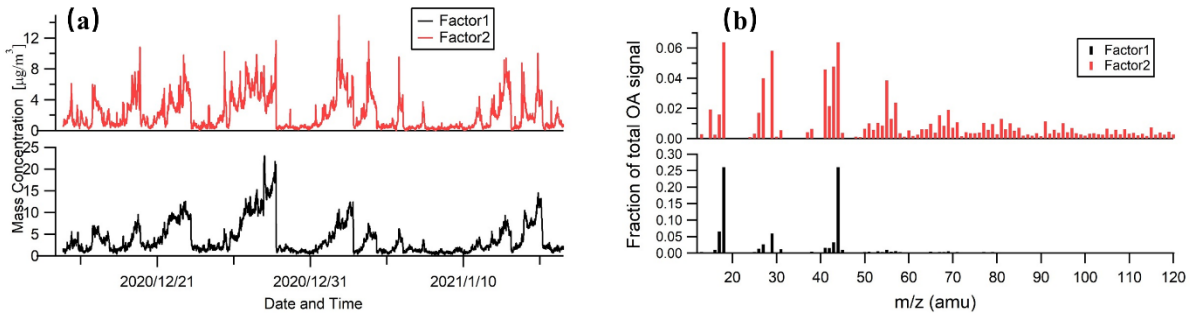

Fig. S2 Time series (a) and mass spectral (b) profiles for the 2-factor PMF solution in PM_1. Factor 1 and factor 2 represent POA and SOA, respectively.

Fig. S3 Summary of key diagnostic plots of the Q-ACSM PMF results for 2-factor resolution

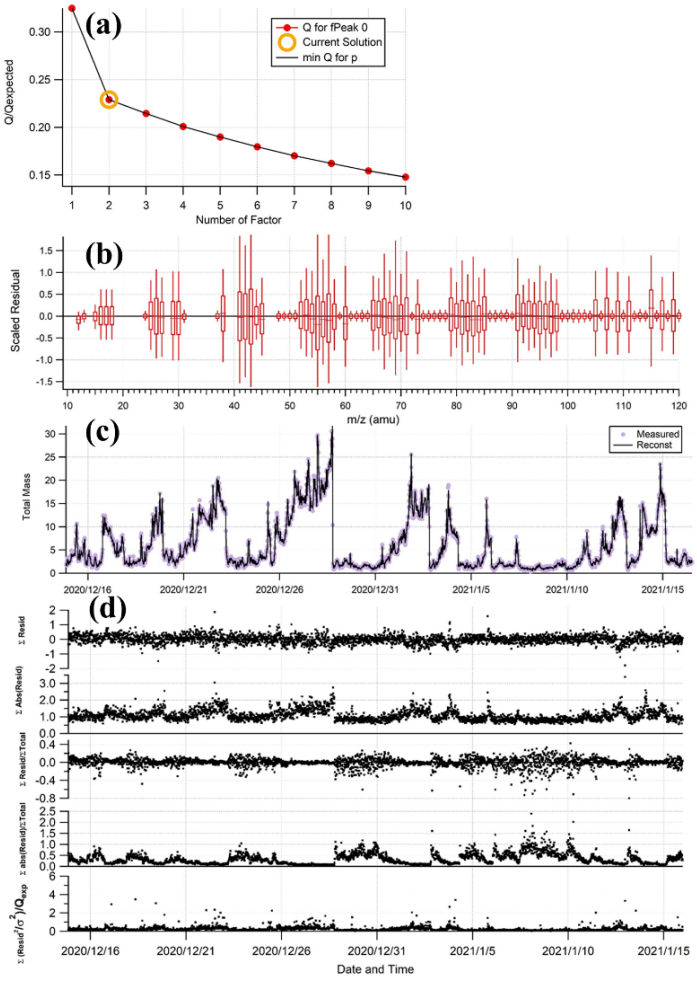

Fig. S3 Summary of key diagnostic plots of the Q-ACSM PMF results for 2-factor resolution: (a) Q/Qexp as a function of number of factors selected for PMF modeling. (b) the box and whiskers plot representing the distribution of OA scaled residuals for each m/z in selected mass spectra. (c) time series of the measured organic mass and the reconstructed OA mass (=POA+SOA). (d) time series of the residual diagnostics and Q/Qexp for each point in time.

Fig. S4 Contribution of organics to total aerosol liquid water content (ALWC)

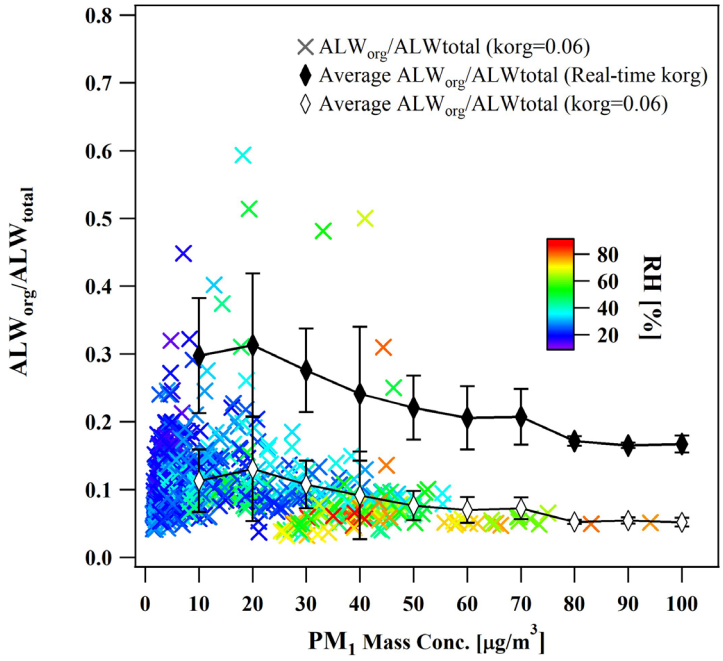

Fig. S4 The colored scatter points represent the mass fraction of ALWC contributed by organics to total ALWC versus the PM_1 mass concentration, which was calculated by mean value of korg=0.06. The color bar represents the ambient RH. The black line with solid and hollow points represents the contribution of average ALWC contributed by organics in total ALWC, which was calculated using average real-time korg and fixded korg.

S3. The unignorable contribution of organics to total ALWC

In this study, the real-time k_{org} was calculated as well with a wide range of f_{44}, which was widely used to represent the atmospheric aging process of OA species (Ng et al., 2010;Canagaratna et al., 2015). In Fig. S4, we considered the variation of real-time f_{44} and calculated the real-time k_{org} to compare the difference on the mass contribution of organics to total ALW between fixed k_{org} and changing k_{org}. k_{org}= 0.06 used in this study was lower than the commonly used k_{org}= 0.1 in other studies (Gysel et al., 2007), but was comparable with the retrieved k_{org} in Beijing varies in the range of 0.06-0.3 (Li et al., 2019;Jin et al., 2020). For fixed k_{org}, the contribution of organics to ALW was ~12% on average during the observation and organics contributed

more on clean days (> 20%) than on polluted days (< 10%). In general, organics with higher f_{44} exhibit larger hygroscopicity (Jimenez et al., 2009;Rickards et al., 2013). Though, the less hygroscopic nature of organics compared to inorganics, the significant fraction of organics to total aerosol mass have impact on total ALW mass. When considering the variation of real-time k_{org} of organics, organics contributed ~29% of the total ALW on average. Organics were capable to provide more than 30% and 20% of the total ALW mass on average during clean days and particulate pollution, respectively. It could be suggested that the increase of oxidation state of organics contributed the overall hygroscopicity of particles. Thus, the promoted hygroscopicity of particles under higher RH condition may increase the ALW mass and worse the air quality. Even though the ALW calculations are different based on several methods (e.g. hygroscopicity tandem differential mobility analyzer (H-TDMA) measurements, the aerosol PNSD under dry and ambient RH conditions, chemical composition closure methods using Zdanovskii-Stokes-Robinson (ZSR) mixing rule and thermal equilibrium models such as ISORROPIA II model) (Kreidenweis and Asa-Awuku, 2014;Gysel et al., 2007;Nguyen et al., 2016;Stanier et al., 2004), which may underestimate or overestimate the ALW contributed by organics (ALW_{org}), the mass fraction of ALW_{org} cannot be ignored irrespective of pollution level in winter Beijing.

Fig. S5 Mass fraction of NR-PM_1 components

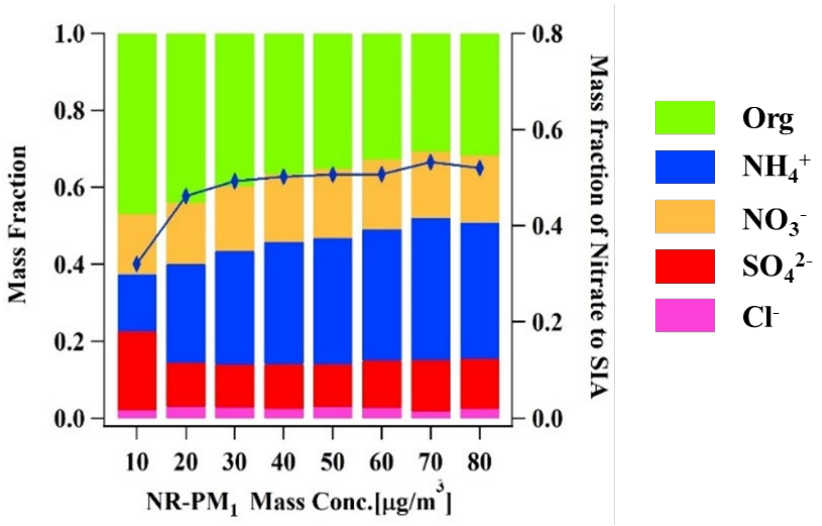

Fig. S5 Mass fraction of NR-PM_1 composition and nitrate to SIA were grouped by the mass

concentration of NR-PM_1.

Fig. S6 Variation of average mass fraction of PM_1 components (NR- PM_1 and ALW) with PM_1 mass concentration

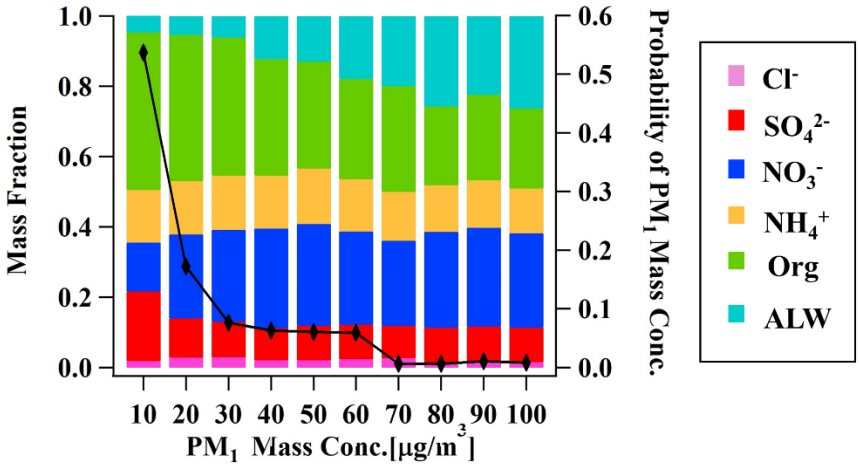

Fig. S6 Variation of average mass fraction of NR-PM_1 and ALW with the PM_1 mass concentration and the probability of PM_1 mass concentration. The black line shows the probability of each PM_1 mass concentration bin.

Fig. S7 Variation of organics components with PM_1 mass concentration

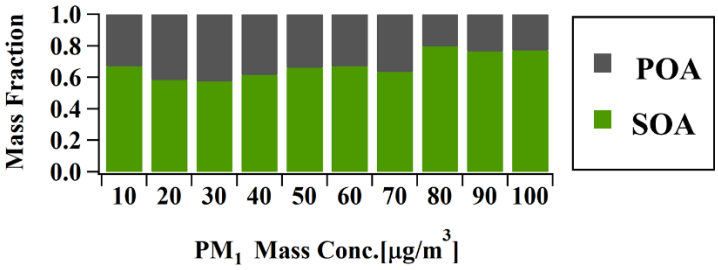

Fig. S7 Variation of average mass fraction of POA and SOA with the increasing PM_1 mass concentration.

S4. Bulk phase viscosity of $PM_{2.5}$ filter samples measured by Poke-and-flow experiments

Poke-and-flow experiments were conducted to determine the semi-solid or solid phases (non-liquid) of $PM_{2.5}$ droplets during clean and polluted days at 293 ± 1 K (Gaikwad et al., 2022;Renbaum-Wolff et al., 2013). As indicated by black and red frame with dashed lines in Fig. 1f, filter samples on Dec 29, 2020 represented the clean day and the others (Dec 21 and

22, 2020 and Jan 1 and 2, 2021) represented the polluted days. Water-soluble species including inorganics and organics in the $PM_{2.5}$ filter samples were extracted in purified water (18.2 MΩ·cm, Millipore, USA). Then, the $PM_{2.5}$ droplets were nebulized on a hydrophobic substrate (Hampton Research, Canada) by a nebulizer and kept in a RH-controlled flow-cell (MEINHARD®, Perkin Elmer, USA) for poke-and-flow experiments.

The procedures of the poke-and-flow experiments have been detailed in previous studies (Renbaum-Wolff et al., 2013;Jeong et al., 2022;Maclean et al., 2021b;Maclean et al., 2021a;Song et al., 2022). Briefly, the initial RH was set at ~100% so that droplets could reach equilibrium, and then the RH was reduced to ~40% at ~1% RH min^{-1}. Then, the droplets were poked at ~40%, ~30%, ~20%, ~10%, or ~0% RH by a needle (Jung Rim Medical Industrial, South Korea) to find the RH at which the droplets started to crack. Before each poking, the droplets were equilibrated for ~1 h at the setpoint RH. Once particles were cracked, they were monitored for ~3 h to check the occurrence of any inflow and outflow using a CCD camera (Hamamatsu, C11440-42U30, Japan). If no flow was detected, the lower limit of viscosity was defined as ~10^8 Pa s (Grayson et al., 2015;Renbaum-Wolff et al., 2013;Song et al., 2019;Maclean et al., 2021b), corresponding to a (semi)solid state. It should be noted that ~10^8 Pa s was the lower limit of viscosity measurement for these $PM_{2.5}$ filter samples by Poke-and-flow technique when no fluid was detected. Thus, (semi)solid, semisolid and liquid conditions were defined within the viscosity range of ~10^8 Pa s, ~10^8 Pa s to ~10^2 Pa s, and ~10^2 Pa s, respectively in this study. Although more precise values were not detected, we can still compare the particle rebound with viscosity range for these aerosols as shown in Fig. S8 and Fig. S9.

Fig. S8 Comparison with online measured-particle rebound fraction and offline measured-viscosity by Poke-and-flow technique

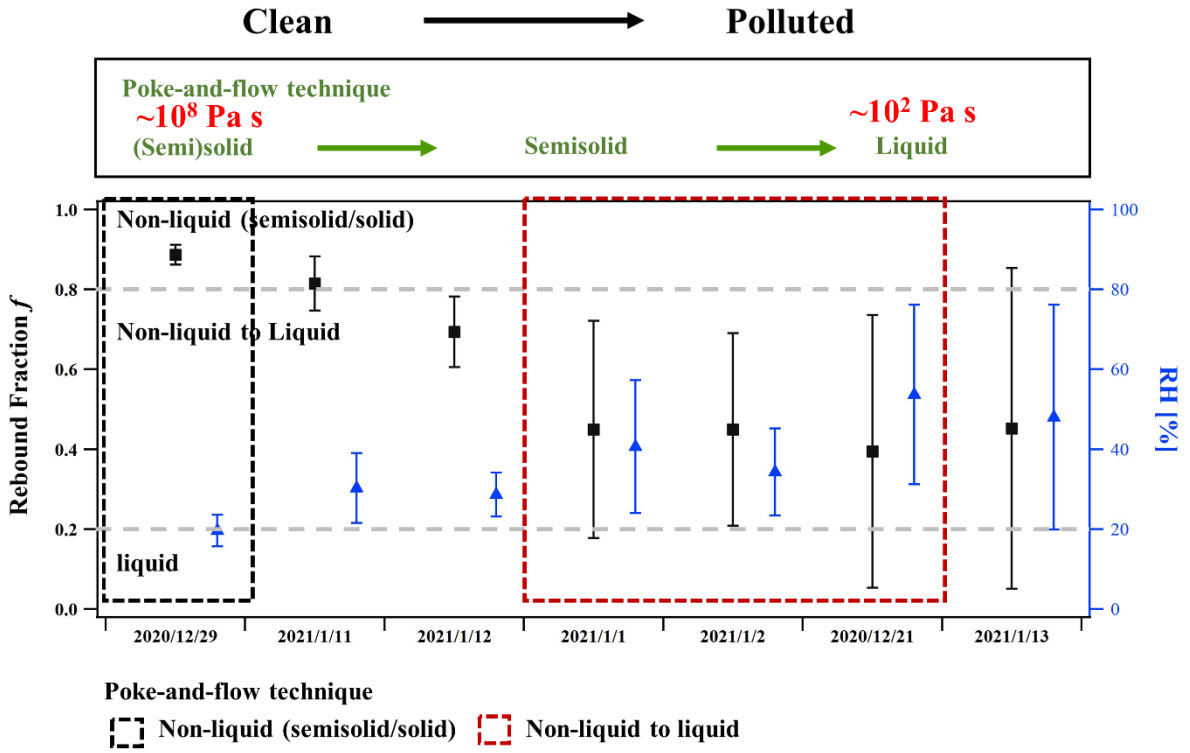

Fig. S8 Averaged particle rebound fraction and ambient RH during filter sampling time for off-line viscosity measurement from clean to polluted days as reported in our previous study (Song et al., 2022). The black and red frames indicate clean day and polluted episodes, which are the same in Fig. 1f. The viscosity results measured by Poke-and-flow technique are shown in the upper frame under certain ambient RH values (mean value of RH). Following our previous study, (semi)solid, semisolid, and liquid are defined as ~10^8 Pa s, ~10^8 - ~10^2 Pa s, and ~10^2 Pa s, respectively.

Fig. S9 Correlation between particle rebound fraction and Poke-and-flow technique measurement for $PM_{2.5}$ filter samples

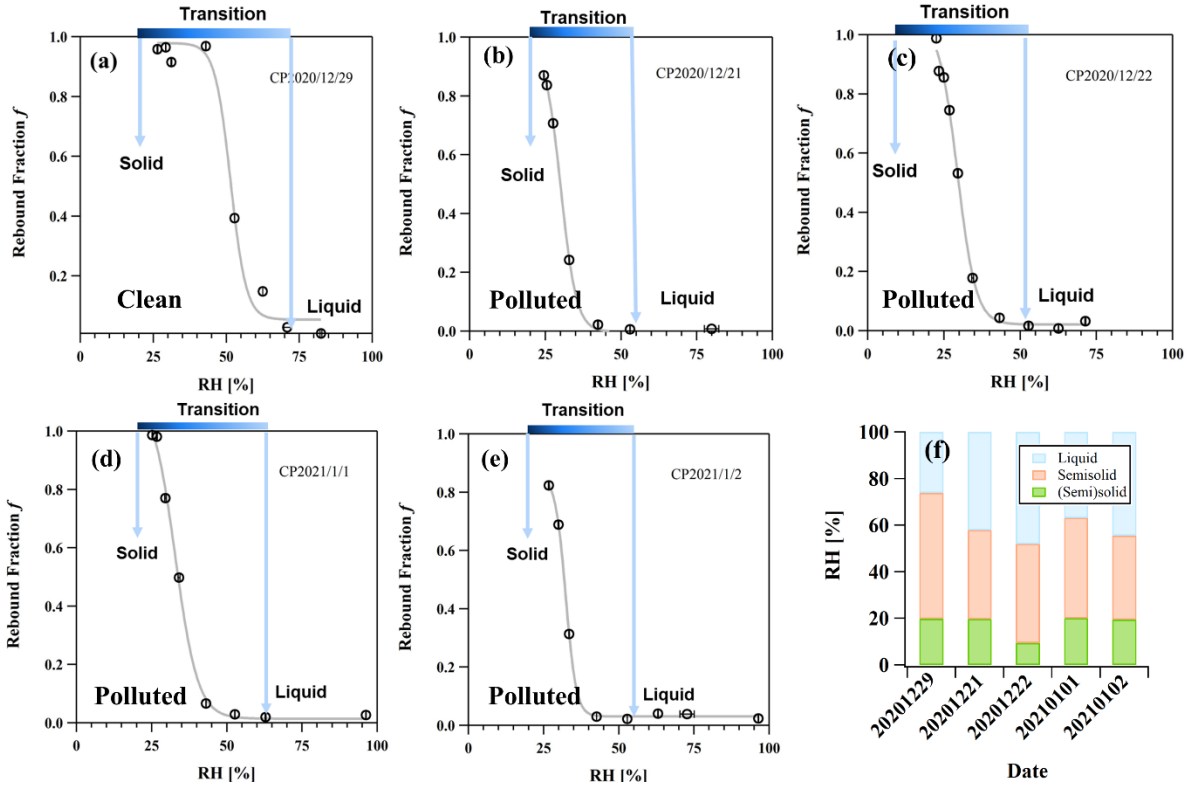

Fig. S9 RH-dependent particle rebound fraction and viscosity range for $PM_{2.5}$ filter samples during clean and polluted days as indicated in Fig. 1f. In panel (f), the RH-dependent viscosity value was the same as our previous report (Song et al., 2022). In the rest panels, the colored blue bars indicate the corresponding RH ranges for the transition from (semi)solid to liquid based on Poke-and-flow technique. (semi)solid, semisolid, and liquid are defined as ~10^8 Pa s, ~10^8 - ~10^2 Pa s, and ~10^2 Pa s, respectively.

S5. Correlation between particle rebound fraction and Poke-and-flow technique measurement for $PM_{2.5}$ filter samples

In order to demonstrate the viscosity variation of phase transition from non-liquid to liquid for the investigated aerosols, we conducted the tests on particle rebound fraction of extracted $PM_{2.5}$ quartz-filter samples with known viscosity as reported above. We extracted these filter samples by the same protocols to get the water-soluble species followed by our previous study (Song et

al., 2022), and regenerated the aerosols by a commercial automizer. Subsequently, the monodisperse aerosols were selected and directly sampled by the three-arm impactor to capture the particle rebound behavior. The particle rebound fraction were measured at decreasing RH levels from 90% to 20% at intervals of 10 min for each RH point, which mimicked the drying process for the determination of (semi)solid and solid phase measurement using the Poke-and-flow technique.

The viscosity range with corresponding RH conditions in panel (f) was illustrated in Fig. S9, while the rested panels showed the RH-dependent particle rebound fraction of these aerosols. As indicated by black and red frame with dashed lines in Fig. 1f, filter samples on Dec 29, 2020 represented the clean day and the others (Dec 21 and 22, 2020 and Jan 1 and 2, 2021) represented the polluted days. The blue bars indicate the corresponding RH range for (semi)solid to liquid phase transition, which was in the viscosity range of ~10^8 Pa s to ~10^2 Pa s. For filter samples on Dec 29, 2020, the ambient RH remained below 30% throughout the sampling period. We observed that particle rebound fraction was ~ 0.0 at RH = 70%, but steadily increased to ~1.0 as the RH decreased to ~45%. Based on the detected RH value of (semi)solid for clean days (~20%), these particles were expected in a more viscous non-liquid state with particle rebound fraction higher than 0.8. For the filter samples on polluted days, the increased rebound fraction along with decreasing RH aligned well with the detected RH range for (semi)solid to liquid transition, indicating that particle rebound fraction with higher values (> 0.8) were expected to indicate the semi-solid or solid state, and phase transition from non-liquid to liquid could be directly inferred from the decreasing rebound fraction from >0.8 to ~ 0.0. Although further detailed validation is still necessary to compare the two different techniques, both the online monitoring of particle rebound behavior during the campaign and the offline measurement of $PM_{2.5}$ filter samples confirmed the consistent phase transition behavior during the polluted periods.

Fig. S10 Particle rebound fraction as a function of aerosol liquid water content

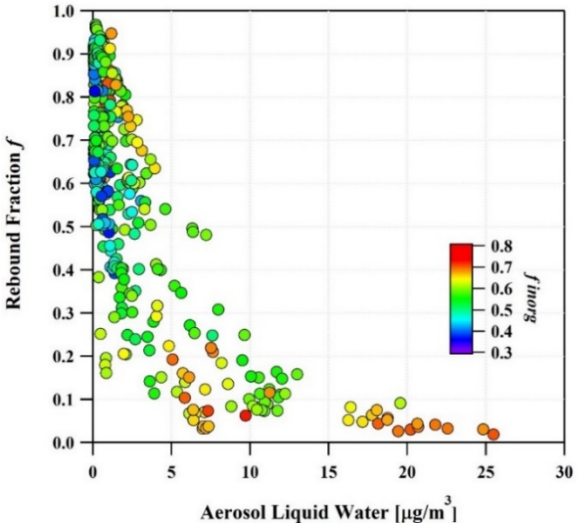

Fig. S10 Particle rebound fraction as a function of aerosol liquid water content during the whole observation in Beijing. The scatter points are colored by the mass fraction of inorganic matter (f_{inorg}) in NR-PM_1.

Fig. S11 A sensitivity analysis of ALW calculation on the phase transition threshold

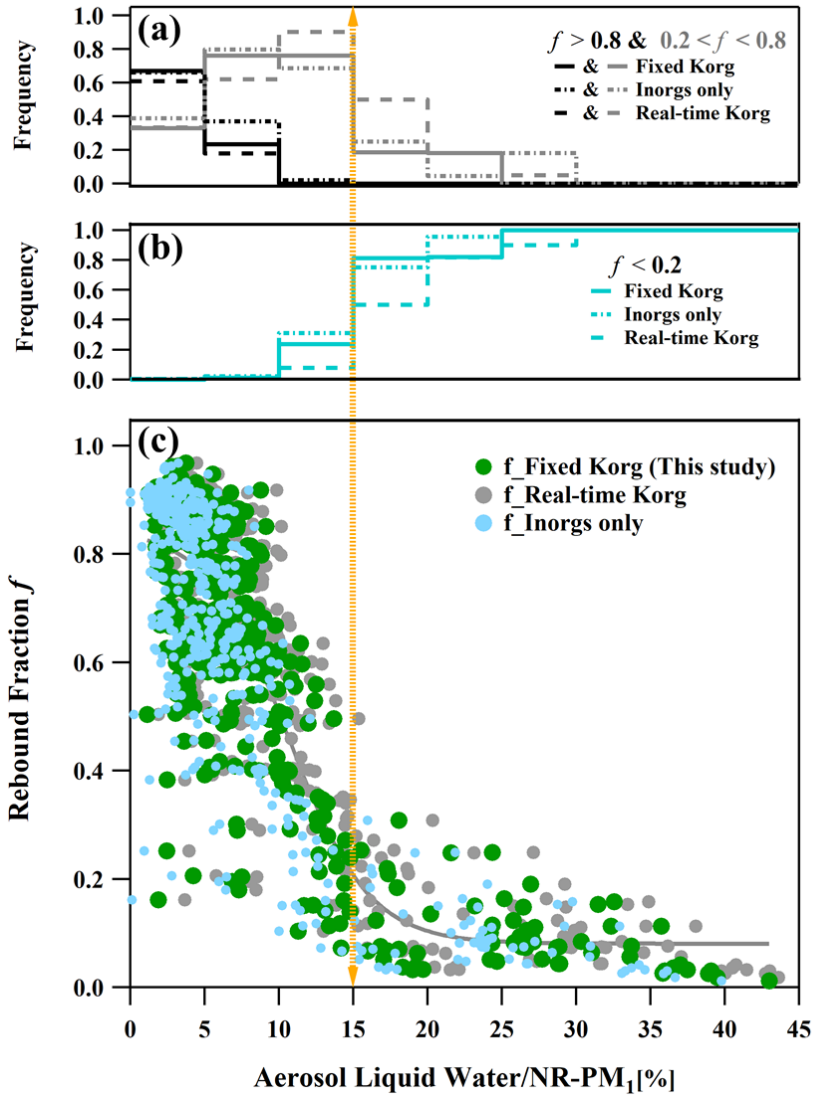

Fig. S11 The frequency distribution of three f intervals (f > 0.8 and $0.2 < f < 0.8$ and f < 0.2) in each ALW/NR-PM_1 bins (a and b) and f as a function of ALW/NR-PM_1 using three different methods of ALW calculation (c).

Fig. S12 The variation of particle rebound fraction during changing RH from high to low conditions

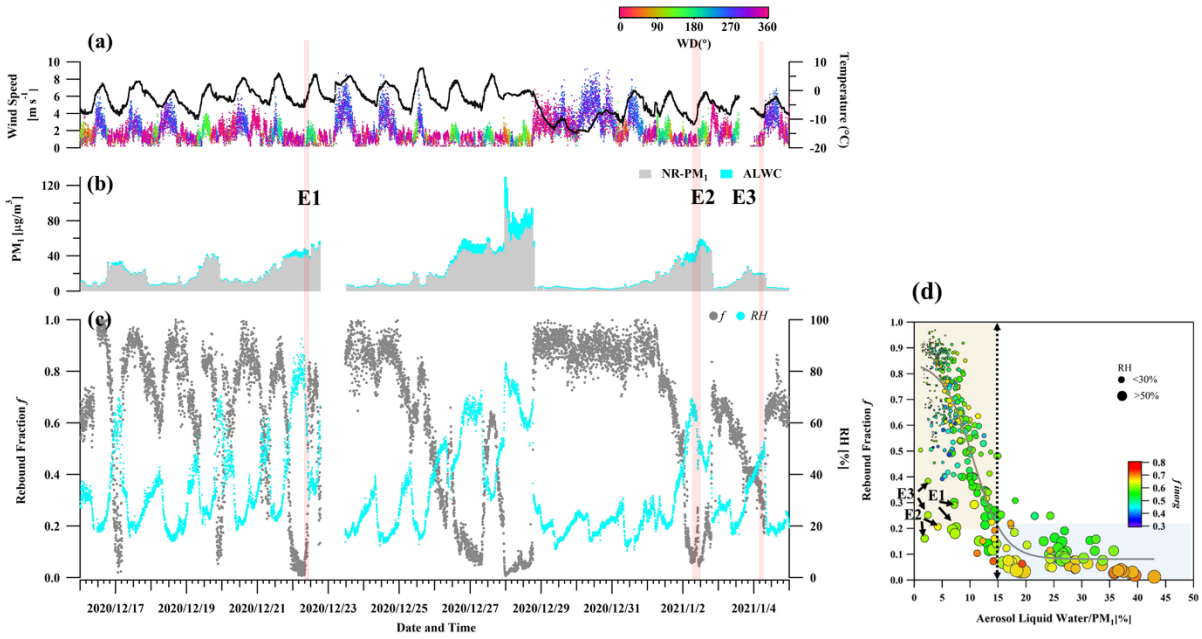

Fig. S12 The variation of particle rebound fraction during changing RH from high to low conditions. Panel (a, b and c) were the same as those in Fig. 1. Panel (d) was similar to Fig. 2d, but particles with lower rebound fraction and ALW/NR-PM_1 < 5% were marked by E1, E2 and E3 with the black arrow and the corresponding periods were indicated by pink shadow in the time series of filed campaign as well.

Fig. S13 Particle rebound fraction dependency of environmental temperature

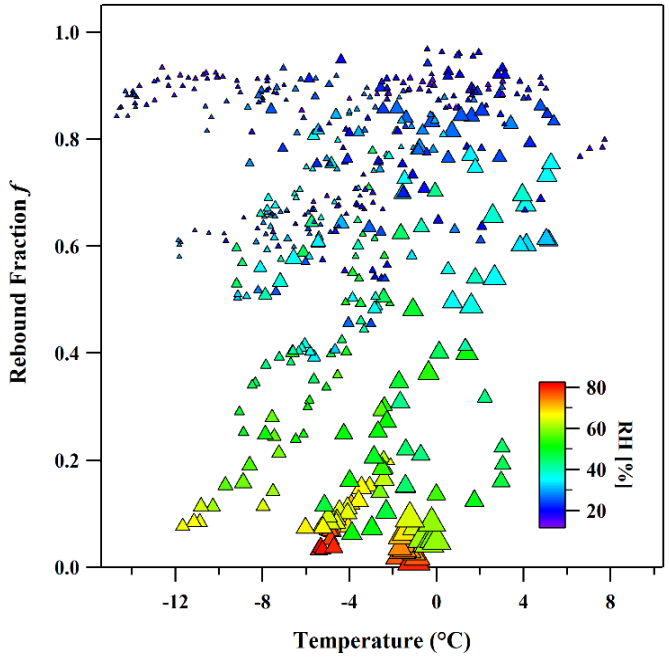

Fig. S13 Particle rebound fraction dependency of environmental temperature. The point size is scaled by NR-PM_1 mass concentration. The points are colored by environmental RH.

S6. Glass transition temperature and viscosity calculations for organic aerosols under ambient conditions

The glass transition temperatures of organic aerosols under dry conditions ($T_{g,org}$) are calculated by the parametrization based on their molecular weight (M) and O:C ratio as below (Shiraiwa et al., 2017):

$$T_g = A + BM + CM^2 + D(O{:}C) + EM(O{:}C), \quad \text{(S1)}$$

Where A=-21.57 K, B=1.51 K mol g^{-1}, C=-1.7×10^{-3} K mol^2 g^{-2}, D=131.4 K and E=-0.25 K mol g^{-1}, respectively. Here, we adopted an average molecular weight of 200 g mol^{-1}, as used in previous studies (Williams et al., 2010;Shen et al., 2018). O:C ratio was calculated by the parametrization of O:C=0.079+4.31×f_{44} (Canagaratna et al., 2015).

The glass transition temperatures of organic-water mixtures (indicate the organic aerosols

under ambient conditions) can be simulated based on the Gordon-Taylor equation (Gordon and Taylor, 1952):

$$T_g(w_{org}) = \frac{(1 - w_{org})T_{g,w} + \frac{1}{k_{GT}} w_{org} T_{g,org}}{(1 - w_{org}) + \frac{1}{k_{GT}} w_{org}}, \quad \text{(S2)}$$

where w_{org} is the mass fraction of OA in the organic-water mixture, $T_{g,w}$ is the glass transition temperature of pure water (136 K), $T_{g,org}$ is the glass transition temperature of OA under dry conditions, and k_{GT} is the Gordon-Taylor constant which is assumed to be 2.5 (Koop et al., 2011). The mass concentration of water in the organic-water mixture is commonly treated as organics-associated water, assuming an externally mixed phase of ambient particles (Shiraiwa et al., 2017;DeRieux et al., 2018;Li et al., 2020). Considering the significant contribution of inorganics to the total ALW mass of ambient aerosols, and the optically undetected liquid-liquid phase separation under staged dehydration of filter-based Beijing $PM_{2.5}$ droplets (Song et al., 2022), we assume in this study that OA particles are internally mixed with inorganic compounds such as sulfate and nitrate. Therefore, we adopted an overall particle hygroscopicity approach to calculate the total ALW mass in the organic-water mixture with the consideration of fixed k_{org} and variable k_{org}. The mass concentration of water of ambient aerosols are calculated, as detailed in Section 2.2.

Then, the viscosity η of ambient OA can be estimated by applying the Vogel–Tammann–Fulcher (VTF) equation (Angell, 1991):

$$\eta = \eta_\infty e^{\frac{T_0 D}{T - T_0}}, \quad \text{(S3)}$$

where η_∞ is the viscosity at infinite temperature (10^{-5} Pa s; Angell, 1991), D is the fragility parameter, which is assumed to be 10 (DeRieux et al., 2018), and T_0 is the Vogel temperature calculated as $T_0 = \frac{39.17 T_g}{D + 39.17}$.

Fig. S14 SOA/POA as a function of rebound fraction during daytime and nighttime

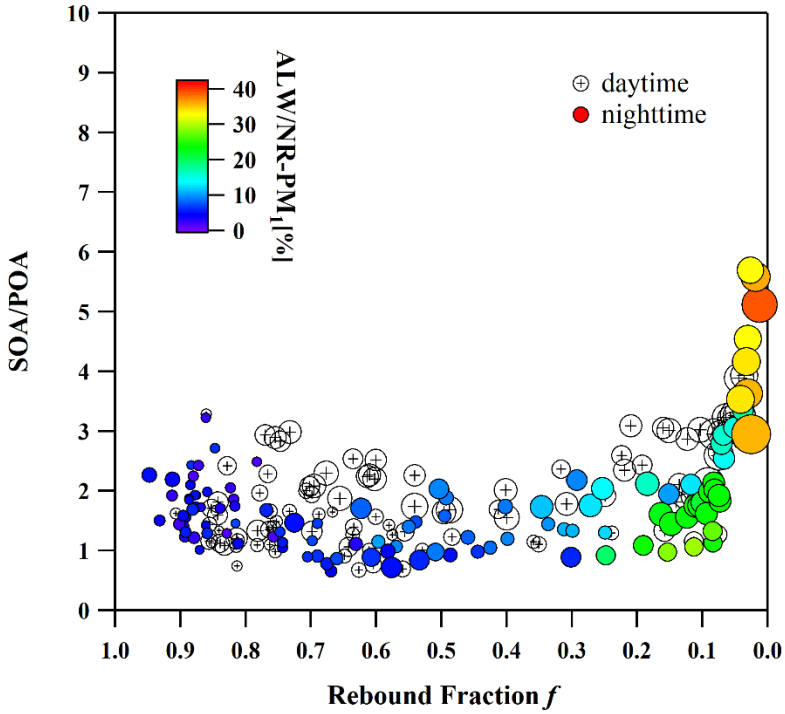

Fig. S14 The relationship between SOA/POA and particle rebound fraction f for phase transition during the daytime (06:00-18:00) and nighttime (18:00-06:00+1 d). The points are colored by ALW/NR-PM_1 to represent the water uptake capacity of the particles. The NR-PM_1 mass concentration is indicated by the size of solid circles.

Fig. S15 The hygroscopicity contributed by organics as a function of RH

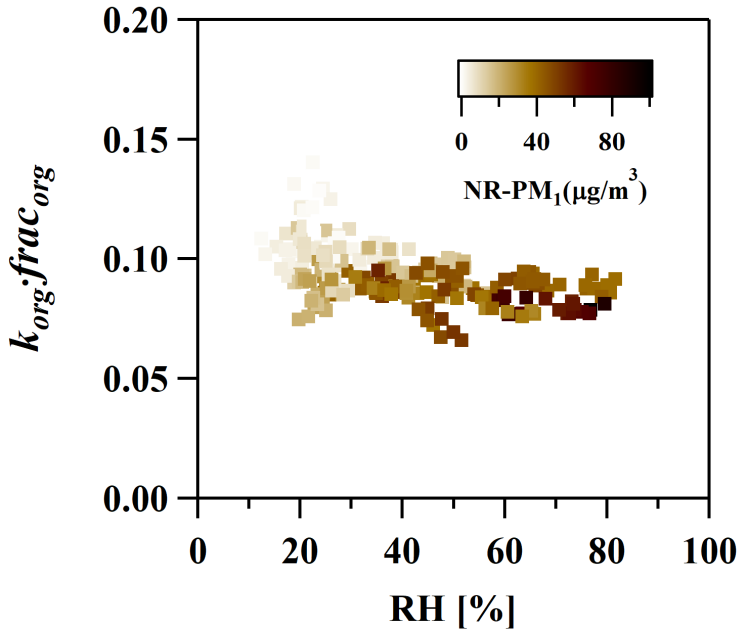

Fig. S15 The hygroscopicity contributed by organics as a function of RH. The hygroscopicity of organics was calculated using real-time f_{44} measured by Q-ACSM. The color bar represents the NR-PM_1 mass concentrations.

Fig. S16 Comparison of aerosol chemical composition, ambient conditions of RH and T, particle phase state and secondary transformation indicators of SIA and SOA for clean and polluted episodes

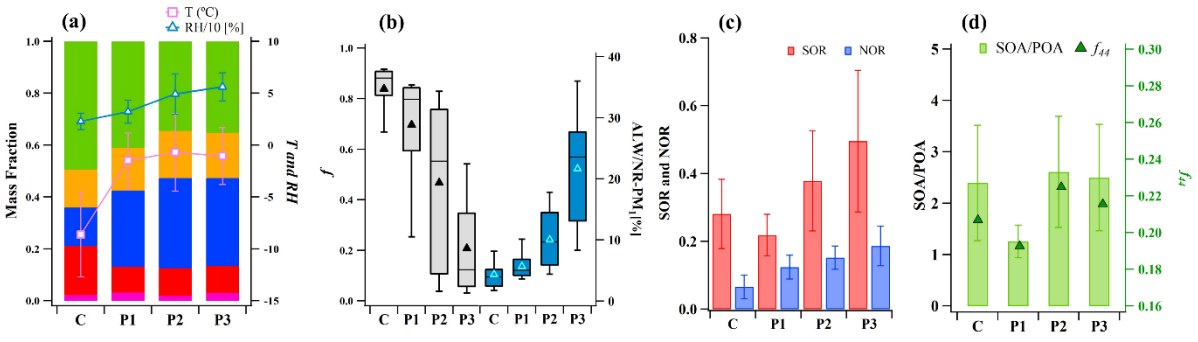

Fig. S16 Changes of aerosol chemical composition, RH and T (a), *f* and ALW/NR-PM_1 (b), SOR and NOR (c), SOA/POA and f_{44} (d) for clean and polluted episodes (P1-P3). In panel (b), the box plots represent the 10th, 25th, 50th, 75th, and 90th percentiles of the corresponding

data. The solid and hollow triangle represents the mean value of the corresponding data for *f* and ALW/NR-PM_1, respectively.

S7. Case studies for polluted episodes during the field observation

Three polluted episodes (P1-P3) and one clean episode were investigated according to aerosol chemical composition, ambient conditions of RH and T, particle phase state and secondary transformation indicators of SIA and SOA. Overall, the polluted episodes had higher RH and T levels than the clean episodes, which favored the accumulation of ALW and associated multiphase processes. The enhanced mass fractions of SIA increased the particle water uptake capacity, leading to the phase transition during polluted episodes. However, phase transition from non-liquid to liquid occurred in P2 and P3 with *f* = ~0.8-0.2 and ALW/NR-PM_1>20% on average. These two polluted episodes had higher secondary transformation rates of SIA and SOA compared to the clean episode and P1 without phase transition, suggesting that phase transition may facilitate the secondary aerosol formation and the haze formation to a certain degree. It is therefore recommended that control strategies for gas pollutant emissions (e.g. SO_2 and NO_x) be implemented to effectively reduce air pollution in China.

Reference

Angell, C. A.: Relaxation in Liquids, Polymers and Plastic Crystals - Strong Fragile Patterns and Problems, J Non-Cryst Solids, 131, 13-31, 1991.

Canagaratna, M. R., Jimenez, J. L., Kroll, J. H., Chen, Q., Kessler, S. H., Massoli, P., Hildebrandt Ruiz, L., Fortner, E., Williams, L. R., Wilson, K. R., Surratt, J. D., Donahue, N. M., Jayne, J. T., and Worsnop, D. R.: Elemental ratio measurements of organic compounds using aerosol mass spectrometry: characterization, improved calibration, and implications, Atmos. Chem. Phys., 15, 253-272, 10.5194/acp-15-253-2015, 2015.

DeRieux, W. S., Li, Y., Lin, P., Laskin, J., Laskin, A., Bertram, A. K., Nizkorodov, S. A., and Shiraiwa, M.: Predicting the glass transition temperature and viscosity of secondary organic material using molecular composition, Atmos Chem Phys, 18, 6331-6351, 2018.

Gaikwad, S., Jeong, R., Kim, D., Lee, K., Jang, K.-S., Kim, C., and Song, M.: Microscopic observation of liquid-liquid-(semi)solid phases in polluted PM2.5, Front., 2022.

Gordon, M., and Taylor, J. S.: Ideal copolymers and the second-order transitions of synthetic rubbers. i. non-crystalline copolymers, Journal of Applied Chemistry, 2, 493-500, 10.1002/jctb.5010020901, 1952.

Grayson, J. W., Song, M., Sellier, M., and Bertram, A. K.: Validation of the poke-flow technique combined with simulations of fluid flow for determining viscosities in samples with small volumes and high viscosities, Atmos. Meas. Tech., 8, 2463-2472, 10.5194/amt-8-2463-2015, 2015.

Gysel, M., Crosier, J., Topping, D. O., Whitehead, J. D., Bower, K. N., Cubison, M. J., Williams, P. I., Flynn, M. J., McFiggans, G. B., and Coe, H.: Closure study between chemical composition and hygroscopic growth of aerosol particles during TORCH2, Atmos. Chem. Phys., 7, 6131-6144, 10.5194/acp-7-6131-2007, 2007.

Jeong, R., Lilek, J., Zuend, A., Xu, R., Chan, M. N., Kim, D., Moon, H. G., and Song, M.: Viscosity and physical state of sucrose mixed with ammonium sulfate droplets, Atmos. Chem. Phys., 22, 8805-8817, 10.5194/acp-22-8805-2022, 2022.

Jimenez, J. L., Canagaratna, M. R., Donahue, N. M., Prevot, A. S. H., Zhang, Q., Kroll, J. H., DeCarlo, P. F., Allan, J. D., Coe, H., Ng, N. L., Aiken, A. C., Docherty, K. S., Ulbrich, I. M., Grieshop, A. P., Robinson, A. L., Duplissy, J., Smith, J. D., Wilson, K. R., Lanz, V. A., Hueglin, C., Sun, Y. L., Tian, J., Laaksonen, A., Raatikainen, T., Rautiainen, J., Vaattovaara, P., Ehn, M., Kulmala, M., Tomlinson, J. M., Collins, D. R., Cubison, M. J., Dunlea, E. J., Huffman, J. A., Onasch, T. B., Alfarra, M. R., Williams, P. I., Bower, K., Kondo, Y., Schneider, J., Drewnick, F., Borrmann, S., Weimer, S., Demerjian, K., Salcedo, D., Cottrell, L., Griffin, R., Takami, A., Miyoshi, T., Hatakeyama, S., Shimono, A., Sun, J. Y., Zhang, Y. M., Dzepina, K., Kimmel, J. R., Sueper, D., Jayne, J. T., Herndon, S. C., Trimborn, A. M., Williams, L. R., Wood, E. C., Middlebrook, A. M., Kolb, C. E., Baltensperger, U., and Worsnop, D. R.: Evolution of Organic Aerosols in the Atmosphere, Science, 326, 1525-1529, 2009.

Jin, X., Wang, Y., Li, Z., Zhang, F., Xu, W., Sun, Y., Fan, X., Chen, G., Wu, H., Ren, J., Wang, Q., and Cribb, M.: Significant contribution of organics to aerosol liquid water content in winter in Beijing, China, Atmos. Chem. Phys., 20, 901-914, 10.5194/acp-20-901-2020, 2020.

Koop, T., Bookhold, J., Shiraiwa, M., and Poschl, U.: Glass transition and phase state of organic compounds: dependency on molecular properties and implications for secondary organic aerosols in the atmosphere, Phys. Chem. Chem. Phys., 13, 19238-19255, 10.1039/c1cp22617g, 2011.

Kreidenweis, S. M., and Asa-Awuku, A.: Aerosol Hygroscopicity: Particle Water Content and Its Role in Atmospheric Processes, 2014,

Li, X. X., Song, S. J., Zhou, W., Hao, J. M., Worsnop, D. R., and Jiang, J. K.: Interactions between aerosol organic components and liquid water content during haze episodes in Beijing, Atmos. Chem. Phys., 19, 12163-12174, 2019.

Li, Y., Day, D. A., Stark, H., Jimenez, J. L., and Shiraiwa, M.: Predictions of the glass transition temperature and viscosity of organic aerosols from volatility distributions, Atmos Chem Phys, 20, 8103-8122, 2020.

Maclean, A. M., Li, Y., Crescenzo, G. V., Smith, N. R., Karydis, V. A., Tsimpidi, A. P., Butenhoff, C. L., Faiola, C. L., Lelieveld, J., and Nizkorodov, S. A.: Global Distribution of the Phase State and Mixing Times within Secondary Organic Aerosol Particles in the Troposphere Based on Room-Temperature Viscosity Measurements, ACS Earth Space Chem, 5, 3458-3473, 2021a.

Maclean, A. M., Smith, N. R., Li, Y., Huang, Y., Hettiyadura, A. P., Crescenzo, G. V., Shiraiwa, M., Laskin, A., Nizkorodov, S. A., and Bertram, A. K.: Humidity-Dependent Viscosity of Secondary Organic Aerosol from Ozonolysis of β-Caryophyllene: Measurements, Predictions, and Implications, ACS Earth Space Chem, 5, 305-318, 2021b.

Ng, N. L., Canagaratna, M. R., Zhang, Q., Jimenez, J. L., Tian, J., Ulbrich, I. M., Kroll, J. H., Docherty, K. S., Chhabra, P. S., Bahreini, R., Murphy, S. M., Seinfeld, J. H., Hildebrandt, L., Donahue, N. M., DeCarlo, P. F., Lanz, V. A., Prevot, A. S. H., Dinar, E., Rudich, Y., and Worsnop, D. R.: Organic aerosol components observed in Northern Hemispheric datasets from Aerosol Mass Spectrometry, Atmos. Chem. Phys., 10, 4625-4641, 10.5194/acp-10-4625-2010, 2010.

Ng, N. L., Herndon, S. C., Trimborn, A., Canagaratna, M. R., Croteau, P. L., Onasch, T. B., Sueper, D., Worsnop, D. R., Zhang, Q., Sun, Y. L., and Jayne, J. T.: An Aerosol Chemical Speciation Monitor (ACSM) for Routine

Monitoring of the Composition and Mass Concentrations of Ambient Aerosol, Aerosol Sci. Technol., 45, 780-794, 10.1080/02786826.2011.560211, 2011.
Nguyen, T. K. V., Zhang, Q., Jimenez, J. L., Pike, M., and Carlton, A. G.: Liquid Water: Ubiquitous Contributor to Aerosol Mass, Environ. Sci. Technol. Lett. , 3, 257-263, 2016.
Price, H. C., Murray, B. J., Mattsson, J., OSulliva n, D., Wilson, T. W., Baustian, K. J., and Benning, L. G.: Quantifying water diffusion in high-viscosity and glassy aqueous solutions using a Raman isotope tracer method, Atmos. Chem. Phys., 14, 3817-3830, 10.5194/acp-14-3817-2014, 2014.
Renbaum-Wolff, L., Grayson, J. W., Bateman, A. P., Kuwata, M., Sellier, M., Murray, B. J., Shilling, J. E., Martin, S. T., and Bertram, A. K.: Viscosity of α-pinene secondary organic material and implications for particle growth and reactivity, Proc. Natl. Acad. Sci., 110, 8014-8019, 2013.
Rickards, A. M. J., Miles, R. E. H., Davies, J. F., Marshall, F. H., and Reid, J. P.: Measurements of the Sensitivity of Aerosol Hygroscopicity and the κ Parameter to the O/C Ratio, The Journal of Physical Chemistry A, 117, 14120-14131, 10.1021/jp407991n, 2013.
Seinfeld, J. H., and Pendis, S. N.: Atmospheric Chemistry and Physics: From Air Pollution to Climate Change, Wiley, 2006.
Shen, H., Chen, Z., Li, H., Qian, X., Qin, X., and Shi, W.: Gas-Particle Partitioning of Carbonyl Compounds in the Ambient Atmosphere, Environmental Science & Technology, 52, 10997-11006, 10.1021/acs.est.8b01882, 2018.
Shiraiwa, M., Li, Y., Tsimpidi, A. P., Karydis, V. A., Berkemeier, T., Pandis, S. N., Lelieveld, J., Koop, T., and Poschl, U.: Global distribution of particle phase state in atmospheric secondary organic aerosols, Nature Communications, 8, 2017.
Song, M., Maclean, A. M., Huang, Y., Smith, N. R., Blair, S. L., Laskin, J., Laskin, A., DeRieux, W.-S. W., Li, Y., Shiraiwa, M., Nizkorodov, S. A., and Bertram, A. K.: Liquid–liquid phase separation and viscosity within secondary organic aerosol generated from diesel fuel vapors, Atmos. Chem. Phys., 19, 12515-12529, 10.5194/acp-19-12515-2019, 2019.
Song, M., Jeong, R., Kim, D., Qiu, Y., Meng, X., Wu, Z., Zuend, A., Ha, Y., Kim, C., Kim, H., Gaikwad, S., Jang, K.-S., Lee, J. Y., and Ahn, J.: Comparison of Phase States of PM2.5 over Megacities, Seoul and Beijing, and Their Implications on Particle Size Distribution, Environ. Sci. Technol. , 10.1021/acs.est.2c06377, 2022.
Stanier, C. O., Khlystov, A. Y., Chan, W. R., Mandiro, M., and Pandis, S. N.: A method for the in situ measurement of fine aerosol water content of ambient aerosols: The dry-ambient aerosol size spectrometer (DAASS), Aerosol Science and Technology, 38, 215-228, 2004.
Williams, B. J., Goldstein, A. H., Kreisberg, N. M., and Hering, S. V.: In situ measurements of gas/particle-phase transitions for atmospheric semivolatile organic compounds, Proceedings of the National Academy of Sciences, 107, 6676-6681, 10.1073/pnas.0911858107, 2010.